X-732-72-196
PREPRINT

NASA TM X-65944

THE SAS-D NUTATION CONTROL SYSTEM

JAVIN M. TAYLOR

JUNE 1972

GSFC
GODDARD SPACE FLIGHT CENTER
GREENBELT, MARYLAND

X-732-72-196

THE SAS-D NUTATION CONTROL SYSTEM

Javin M. Taylor

NASA-ASEE Summer Faculty Fellow

June 1972

Goddard Space Flight Center
Greenbelt, Maryland

CONTENTS

ILLUSTRATIONS

THE SAS-D NUTATION CONTROL SYSTEM

Javin M. Taylor

NASA-ASEE Summer Faculty Fellow

ABSTRACT

A control law is developed for the SAS-D nutation control system. Nutation is removed in a sub-optimal manner with respect to fuel consumed, but attitude errors are minimized.

The research performed consists of an investigation of nutation theory and nutation due to energy dissipation, nutation detection analysis, nutation control analysis, and error analysis. The resulting nutation control system uses an accelerometer or rate gyro to sense the nutation angle θ which varies sinusoidally at the nutation frequency Ω. The sensed nutation angle is compared with a threshold θ_T. If the sensed nutation is greater, a thrust pulse of duration equal to the period of one spin cycle is initiated. Since the threshold θ_T is set equal to the amount of nutation that can be removed by one thrust pulse of duration equal to one spin cycle, the spacecraft nutation is reduced to near zero.

Error analysis indicates that the nutation sensed, the threshold, the amount of nutation that can be removed during one thrust pulse, and the time duration of one thrust pulse are all sensitive to the spacecraft spin frequency imparted by the Delta rocket. Thus, the nutation control system was designed to be adaptive to the possible variations in imparted spin frequency.

THE SAS-D NUTATION CONTROL SYSTEM

INTRODUCTION

This report describes the Phase B study of the active nutation control for the SAS-D spacecraft. Following Grasshoff [1], the theory of nutation control for a asymmetrical vehicle, such as the SAS-D, is developed. Then an engineering analysis is performed which evaluates various nutation sensor schemes and nutation control schemes. Specifically, nutation sensing methods using an accelerometer, a rate gyro, or a pre-positioned rate gyro are developed. Then, a nutation control law is developed and an error analysis performed.

Nutation control is required because of energy dissipation within a spin stabilized spacecraft spinning about an unfavorable inertia axis. The energy dissipation time constant is the critical parameter in designing the active nutation control system. Preliminary analysis by other investigators predicts an energy dissipation time constant for the SAS-D spacecraft of greater than 10,000 seconds. However, since assuming a large time constant and experiencing a much smaller one can prove disastrous, this analysis assumes a time constant of 500-1000 seconds. This conservative design will still be valid if future analysis and simulation substantiate the large time constant.

NUTATION THEORY

The rate of nutation Ω and nutation angle θ can be derived from the basic equations for a rotating body

$$\dot{\mathbf{H}} = \mathbf{M} \tag{1}$$

where $\mathbf{H}$ is the total angular momentum and $\mathbf{M}$ is the total applied torque. Furthermore, considering motion in a moving reference frame described by

$$\dot{\mathbf{H}}_{MOV} = \dot{\mathbf{H}}_{REL} + \omega \times \mathbf{H}_{MOV} \tag{2}$$

where ω is the total angular velocity, and selecting the axis system to be the principle axes so that

$$\mathbf{H} = \mathbf{I}\,\omega = \begin{bmatrix} I_x\,\omega_x \\ I_y\,\omega_y \\ I_z\,\omega_z \end{bmatrix} \tag{3}$$

where I is the total inertia, the equation of motion becomes

$$\mathbf{I}\,\dot{\omega} + \omega \times (\mathbf{I}\,\omega) = \mathbf{M}. \tag{4}$$

$$\begin{bmatrix} I_x\,\dot{\omega}_x \\ I_y\,\dot{\omega}_y \\ I_z\,\dot{\omega}_z \end{bmatrix} + \begin{bmatrix} \omega_y\,I_z\,\omega_z - \omega_z\,I_y\,\omega_y \\ \omega_z\,I_x\,\omega_x - \omega_x\,I_z\,\omega_z \\ \omega_x\,I_y\,\omega_y - \omega_y\,I_x\,\omega_x \end{bmatrix} = \begin{bmatrix} M_x \\ M_y \\ M_z \end{bmatrix} \tag{5}$$

Defining the spin axis of the SAS-D to be the x-axis and assuming $\dot{\omega}_x = 0$, the remaining differential equations can be written in the form

$$\begin{aligned} \dot{\omega}_y - \left[\left(\frac{I_z}{I_y} - \frac{I_x}{I_y}\right)\omega_x\right]\omega_z &= \frac{M_y}{I_y} \\ \dot{\omega}_z + \left[\left(\frac{I_y}{I_z} - \frac{I_x}{I_z}\right)\omega_x\right]\omega_y &= \frac{M_z}{I_z} \end{aligned} \tag{6}$$

or

$$\begin{aligned} \dot{\omega}_y - \Omega_y\,\omega_z &= \frac{M_y}{I_y} \\ \dot{\omega}_z + \Omega_z\,\omega_y &= \frac{M_z}{I_z} \end{aligned} \tag{7}$$

Following Grasshoff [1], and using complex variables notation, the differential equation for the transverse angular velocity can be expressed as

$$\dot{\omega}\,(t) + i\,\Omega\,\omega\,(t) = N \tag{8}$$

where

$$\omega\,(t) = \omega_y\,(t) + i\left(\frac{\Omega_y}{\Omega_z}\right)^{1/2}\omega_z\,(t), \tag{9}$$

$$\Omega = \pm (\Omega_y \, \Omega_z)^{1/2} \text{ (sign positive for SAS-D)}, \tag{10}$$

$$N = \frac{M_y}{I_y} + i \left(\frac{\Omega_y}{\Omega_z} \right) \frac{M_z}{I_z}. \tag{11}$$

Thus, if the solution for equation (8) is non-zero, nutation, consisting of a nutation frequency Ω and nutation angle θ, exists.

Following Timoshenko and Young [2], the nutation motion can be described by a body cone moving around a space cone, as shown in Figure 1.

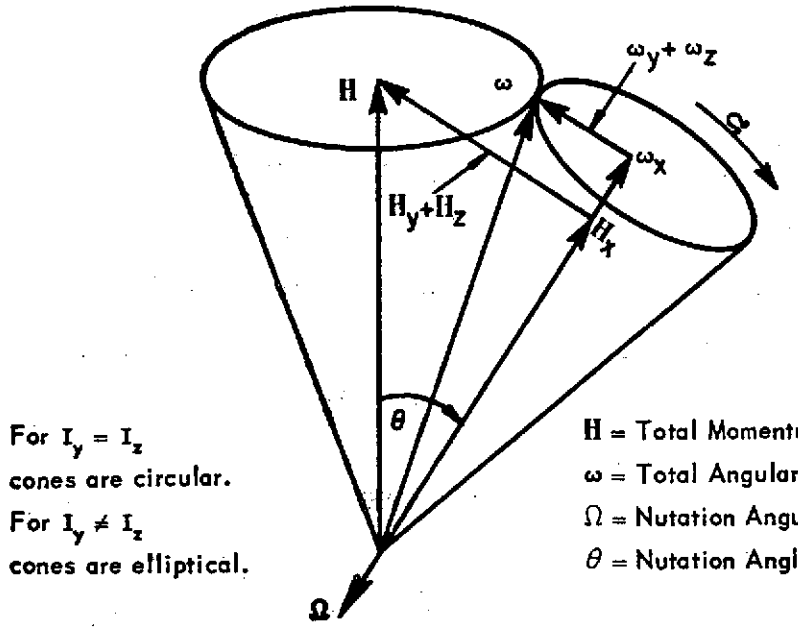

Figure 1. Nutation Motion.

For the initial condition $\omega_0 = \omega(0)$, the torque-free solution of equation (8) is given by

$$\omega(t) = \omega_0 \, e^{-i\Omega t} \tag{12}$$

Substituting equation (9) into equation (12),

$$\omega(t) = \left[\omega_{y0} + i \left(\frac{\Omega_y}{\Omega_z} \right)^{1/2} \omega_{z0} \right] e^{-i\Omega t} \tag{13}$$

Assuming zero phase reference

$$\omega(t) = A_y \sin \Omega t + i \left(\frac{\Omega_y}{\Omega_z}\right)^{1/2} A_z \cos \Omega t \tag{14}$$

where

$$A_y = \left[\omega_{y0}^2 + \left(\frac{\Omega_y}{\Omega_z}\right)\omega_{z0}^2\right]^{1/2} \tag{15}$$

$$A_z = \left[\omega_{y0}^2 \Big/ \left(\frac{\Omega_y}{\Omega_z}\right) + \omega_{z0}^2\right]^{1/2} \tag{16}$$

and letting $(\Omega_y/\Omega_z)^{1/2} = k$, then

$$A_y = k\, A_z \tag{17}$$

From Figure 1, for small angles the nutation angle θ is defined to be

$$\theta = \tan\theta = \frac{[H_y^2 + H_z^2]^{1/2}_{max}}{H_x} \tag{18}$$

which reduces to

$$\theta = \frac{A_z}{\omega_x - \Omega} \tag{19}$$

Returning to equation (8), the complete solution for the differential equation is given by

$$\omega(t) = \omega_0\, e^{-i\Omega(t-t_0)} + \frac{N}{i\,\Omega}\left[1 - e^{-i\Omega(t-t_0)}\right] \tag{20}$$

Now, let the torque N be defined as

$$N = N_0\, e^{i\lambda} \tag{21}$$

where λ is measured ccw from the SAS-D y-axis.

For a torque applied for $(t_1 - t_0)$ seconds, $\omega(t_1)$ is given by

$$\omega(t_1) = \omega_0 e^{-i\Omega(t_1 - t_0)} + \frac{N_0 e^{i\lambda}}{i\Omega}\left[1 - e^{-i\Omega(t_1 - t_0)}\right] \tag{22}$$

and through trigonometric manipulation

$$\omega(t_1) = \omega_0 e^{-i\Omega(t_1 - t_0)} + \frac{2N_0}{\Omega} \sin\left[\frac{\Omega(t_1 - t_0)}{2}\right] e^{i[\lambda - \Omega/2(t_1 - t_0)]} \tag{23}$$

The magnitude of $\omega(t_1)$ is given by

$$|\omega(t_1)| = \left| \omega_0 e^{-i\Omega(t_1 - t_0)} + \frac{2N_0}{\Omega} \sin\left[\frac{\Omega(t_1 - t_0)}{2}\right] e^{i[\lambda - \Omega/2(t_1 - t_0)]} \right| \tag{24}$$

From equation (24), the magnitude of $\omega(t_1)$ will be minimized with respect to λ if the torque N_0 is applied 180° from $\omega_0 e^{-i\Omega(t_1 - t_0)}$. Thus,

$$\lambda - \frac{\Omega(t_1 - t_0)}{2} = \pi - \Omega(t_1 - t_0) \tag{25}$$

$$\lambda = \pi - \frac{\Omega(t_1 - t_0)}{2} \tag{26}$$

Furthermore, after obtaining the optimum torque angle from equation (26), the torque duration is maximized if

$$\frac{\Omega(t_1 - t_0)}{2} = \pi/2, \tag{27}$$

i.e.,

$$(t_1 - t_0) = 1/2\, T_\Omega \tag{28}$$

where T_Ω is the period of the nutation frequency. Thus, maximum nutation is removed during each nutation cycle if the torque is aligned as in equation (26) and the torque duration from equation (28) is one-half a nutation cycle.

Returning to equation (24) let $\Delta\omega_0$ be defined by

$$\Delta\omega_0 = \frac{2N_0}{\Omega} \sin\left[\frac{\Omega(t_1 - t_0)}{2}\right] \tag{29}$$

which for proper choice of λ is the maximum change in the transverse angular velocity $\omega(t)$. From Equation (19), the maximum change in the nutation angle is

$$\Delta\theta = \frac{-\Delta\omega_0}{\omega_x - \Omega} \tag{30}$$

To summarize, equation (29) shows the amount of transverse angular velocity that can be removed so that in equation (22), $\omega(t_1)$ is less than ω_0. Furthermore, since energy dissipation exists in the spin stabilized SAS-D, the transverse angular velocity tends to increase and must periodically be reduced through the use of nutation control. Increase in nutation due to energy dissipation is discussed in the next section.

Table 1 presents the analysis data for the SAS-D nutation control system. Lines 1-11 are the result of the material developed in this section. Nutation control will possibly be required during three parts of the spacecraft trajectory. These parts are: segment A, the transfer ellipse; segment B, after apogee burn; segment C, during synchronous orbit trim. Hence, the three columns in Table 1.

NUTATION DUE TO ENERGY DISSIPATION

Spin stabilization of the SAS-D spacecraft about an axis other than that of maximum inertia results in a possibly unstable stability condition. Energy dissipation due to fluid motion in heat pipe and fuel tanks causes the nutation angle to increase until the stable condition of spin about the maximum inertia axis is reached. To counteract this condition, the nutation control system must add energy to compensate for the energy dissipated.

It is generally accepted that for small perturbations the increase in nutation angle due to energy dissipation is exponential and of the form

$$\theta(t) = \theta_0 e^{t/\tau} \tag{30}$$

Table 1
Analysis Data for SAS-D Nutation Control

Item No.	Parameter	Segment A	Segment B	Segment C	Comment
1	I_x	70.9	62.4	60.3	Fig. 5.8-1, Phase A Report, units are slug ft^2
2	I_y	211.8	156.3	151.0	
3	I_z	216.7	160.8	155.5	
4	$\Omega_y(\omega_x)$	$0.6884\omega_x$	$0.6296\omega_x$	$0.6305\omega_x$	Calculated with ω_x as a parameter
5	$\Omega_z(\omega_x)$	$0.6502\omega_x$	$0.5839\omega_x$	$0.5833\omega_x$	
6	$\Omega(\omega_x)$	$0.6690\omega_x$	$0.6063\omega_x$	$0.6064\omega_x$	
7	k	1.0290	1.0384	1.0397	$k = [\Omega_y/\Omega_z]^{1/2}$
8	ω_x	1.0 rev/sec	1.0 rev/sec	1.0 rev/sec	Range is 1.0 rev/sec ±20%
9	$\Omega(1.0)$	0.6690	0.6063	0.6064	Units are rev/sec
10	$T_\Omega(1.0)$	1.4948 sec	1.6493 sec	1.6491 sec	
11	N_0	0.0673	0.0895	0.0924	Units are lb-sec^2-ft.
12	σ_y	0.3347	0.3992	0.3993	$\sigma_y = I_x/I_y$
13	σ_z	0.3272	0.3881	0.3878	$\sigma_z = I_x/I_z$
14	τ_y	31.552 sec 8.76 hr 34,968 sec	12,359 sec 3.44 hrs 14,144 sec	11,963 sec 3.32 hrs 13,713 sec	Energy dissipation time constant
15	τ_z	9.71 hrs	3.93 hrs	3.81 hrs	
16	ϕ_A	30.4°	19.1°	19.1°	Nominal accelerometer position
17	$\lvert a_x \rvert$	3.47 r θ	3.97 r θ	3.97 r θ	Accelerometer output magnitude
18	ϕ_{RG}	30.4°	19.1°	19.1°	Nominal rate gyro position
19	$\lvert \omega_M \rvert$	2.94 θ	3.49θ	3.49θ	Rate gyro output magnitude
20	ψ_{RG}	-59.55°	-70.84°	-70.84°	Nominal phase for pre-positioned rate gyro
21	$\lvert \omega_M \rvert$	2.14 θ	2.57θ	2.57 θ	Pre-positioned rate gyro output magnitude

Table 1–(continued)

Item No.	Parameter	Segment A	Segment B	Segment C	Comment
22	$\Delta\theta_{\omega_x}$	-0.7715°	-0.7839°	-0.8183°	Thrust duration is one spin cycle
23	T_N	2303 sec	1152 sec	1152 sec	Time between thrust pulses
24	H_N	1.833 lbs.	0.1 lbs.	0.76 lbs.	Hydrazine reg'd for nutation control
25	$\Delta\theta_{opt}$	-0.8752°	-1.0490°	-1.0813°	Maximum θ that can be removed
26	Max $\theta_{\omega x}$	515°	237°	247°	
27	Max θ_{opt}	585°	317°	327°	
28	τ	1000 sec	500 sec	500 sec	Conservative estimate of energy dissipation time constant

where τ is the time constant of energy dissipation in the spacecraft.

In "Phase A Report for Small UV Astronomy Satellite," τ is calculated to be on the order of 20,000 seconds. However, because of the inadequate theoretical and experimental knowledge at this time, a time constant of 20,000 seconds is viewed with great skepticism. Thus, the energy dissipation time constant used in this report will be very conservative and on the order of 500-1,000 seconds.

Following Fedor's memo [4], which uses the energy sink approach, the time constant due to the heat pipes for small nutation angles is given by

$$\tau = \frac{4\, I_T\, (1-\sigma)}{m\, \omega_s\, \Sigma\, z_i^2\, \sigma^3} \tag{31}$$

where

σ - ratio of rotational to transverse interias for symmetric body. For SAS-D, $\sigma = I_x/I_T$

I_T - transverse inertia for symmetric body.

m - mass of fluid in heat pipes.

Σz_i^2 - summation of heat pipe locations.

ω_s - spacecraft spin. $\omega_s = \omega_x$

Using the parameters given in the Phase A report [3], page 5-69, for m and Σz_i^2, τ ranges from about 12,000 to 32,000 seconds. (See items 12-15, Table 1.)

Even if the energy dissipation due to fluid movement in the spacecraft is well understood, the time constant τ varies greatly for small changes in the inertia ratio σ. Since σ will probably change during the course of the SAS-D program, an analysis of variation in τ due to σ is warranted. Thus, the Taylor's series expansion of equation (31) about the nominal inertia ratio σ_0, with higher order terms ignored, yields

$$\tau \simeq \frac{4 I_T}{m \omega_s \Sigma z_i^2} \left[\left(\frac{1 - \sigma_0}{\sigma_0^3} \right) + \frac{d}{d\sigma} \left(\frac{1 - \sigma}{\sigma^3} \right)_{\sigma = \sigma_0} \delta \sigma \right] \tag{32}$$

By allowing the approximation

$$3 - 2\sigma_0 \simeq 3 (1 - \sigma_0) \tag{33}$$

and simplifying, the final result is

$$\tau \simeq \frac{4 I_T}{m \omega_s \Sigma z_i^2} \left(\frac{1 - \sigma_0}{\sigma_0^3} \right) \left[1 - \frac{3 \delta \sigma}{\sigma_0} \right] \tag{34}$$

$$\tau \simeq \tau_0 \left[1 - 3 \frac{\delta \sigma}{\sigma_0} \right] \tag{35}$$

Thus, for example, a change in σ from 0.330 to 0.397 (see Table 1, line 12, segments A and B), that is, 20%, results in a new time constant approximately 40% of its original value. (See Table 1, line 14, segments A and B.) This fact reiterates the need to assume a conservative time constant at this point in the program.

The increase in nutation angle described by equation (30) is valid for small values of θ. Alfried [5] indicates that the exponential increase in nutation angle changes to the form

$$\theta(t) = \theta_0 \sqrt{1 - \frac{t}{\tau'}} \tag{35}$$

where τ' is a different time constant from τ. Here the nutation angle builds up faster than in equation (30).

Furthermore, Alfriend gives the relation for the crossover from behavior described by equation (30) to equation (35) by

$$\theta = \frac{(\sigma - 1)\,\eta}{b\,\sigma\,\Omega} \tag{36}$$

where

σ - ratio of rotational to transverse inertia

η - damping coefficient

b - heat pipe height to radius ratio

Ω - nutation frequency.

Without going into the detail, rough calculations indicate that θ can build up about 15° before equation (35) is applicable.

NUTATION DETECTION

The SAS-D nutation can be detected using several methods. In this report nutation detection using an accelerometer or a rate gyro will be discussed.

Accelerometer. To detect nutation using an accelerometer consider the acceleration at a point located $\rho = \text{col}\,[x_0\ y_0\ z_0]$ from the spacecraft c.g. The acceleration experienced at this point is

$$\mathbf{a} = \dot{\boldsymbol{\omega}} \times \boldsymbol{\rho} + \boldsymbol{\omega} \times (\boldsymbol{\omega} \times \boldsymbol{\rho}) \tag{37}$$

which reduces to

$$\begin{bmatrix} a_x \\ a_y \\ a_z \end{bmatrix} = \begin{bmatrix} \dot{\omega}_y z_0 - \dot{\omega}_z y_0 \\ \dot{\omega}_z x_0 - \dot{\omega}_x z_0 \\ \dot{\omega}_x y_0 - \dot{\omega}_y x_0 \end{bmatrix} + \begin{bmatrix} \omega_y (\omega_x y_0 - \omega_y x_0) + \omega_z (\omega_x z_0 - \omega_z x_0) \\ \omega_x (\omega_y x_0 - \omega_x y_0) + \omega_z (\omega_y z_0 - \omega_z y_0) \\ \omega_x (\omega_z x_0 - \omega_x z_0) + \omega_y (\omega_z y_0 - \omega_y z_0) \end{bmatrix} \tag{38}$$

For an accelerometer mounted at $x_0 = 0$ with its input axis parallel to the principle x-axis,

$$a_x = (\omega_y \omega_x - \dot{\omega}_z) y_0 + (\omega_z \omega_x + \dot{\omega}_y) z_0 \tag{39}$$

Using the results of equations (9) and (14) that

$$\omega_y = A_y \sin \Omega t$$

$$\omega_z = A_z \cos \Omega t$$

equation (39) becomes

$$a_x = (A_y \omega_x + A_z \Omega) y_0 \sin \Omega t + (A_z \omega_x + A_y \Omega) z_0 \cos \Omega t \tag{40}$$

Again, following Grasshoff [1] and using phase notation, let

$$a_x = a_0 \theta \sin (\Omega t + \phi), \tag{41}$$

$$a_0 = [\{(k \omega_x + \Omega) y_0\}^2 + \{(\omega_x + k \Omega) z_0\}^2]^{1/2} (\omega_x - \Omega), \tag{42}$$

and

$$\phi = \tan^{-1} \left[\frac{(\omega_x + k \Omega) z_0}{(k \omega_x + \Omega) y_0} \right] \tag{43}$$

Here ϕ is measured ccw from the positive principle y-axis. Thus, from equation (41) the acceleration sensed is proportional to the nutation angle θ and is sinusoidal at the nutation frequency rate, with phase shift ϕ.

The phase in equation (43) depends upon the position of the accelerometer. Thus, it is possible to place the accelerometer so that if the thruster is actuated at some phase with respect to the maximum acceleration sensed, the nutation of equation (24) will decrease. Let equation (41) be modified to the form

$$a_x = a_0 \theta \sin (\Omega t + \mu) \tag{44}$$

and

$$\mu = \phi + \psi + \beta_T \tag{45}$$

where

ψ - total phase shift due to electrical hardware.

β_T - phase advancement to compensate for position of thrust centroid.

Now, for optimum nutation removal, μ should be set equal to the optimum phase in equation (26). Hence,

$$\mu = \lambda - \pi + \Omega\left(\frac{t_1 - t_0}{2}\right) \tag{46}$$

From equation (45),

$$\phi + \psi + \beta_T = \lambda - \pi + \Omega\left(\frac{t_1 - t_0}{2}\right) \tag{47}$$

$$\phi = \lambda - \pi - \psi + \left[\Omega\left(\frac{t_1 - t_0}{2}\right) - \beta_T\right] \tag{48}$$

Substituting equation (48) into equation (43) the position of the accelerometer is

$$\frac{z_0}{y_0} = \left[\frac{k\,\omega_x + \Omega}{\omega_x + k\,\Omega}\right] \tan\phi \tag{49}$$

Thus, the angular position of the accelerometer is given by

$$\tan\phi_A = \frac{z_0}{y_0} \tag{50}$$

where ϕ_A is measured ccw from the positive principle y-axis.

For the SAS-D vehicle, nutation control will be accomplished by the two 5-lb thrusters, with three foot moment arms, mounted on the plus and minus y-axis. Thus, $\lambda = \pm\pi/2$. Furthermore, assume that ψ, $\beta_T = 0$ in equation (48).

Also, assume that the applied thrust pulse will be the duration of one spin cycle, i.e., one second for a nominal $\omega_x = 1.0$ rev/sec. From equation (48), for $\lambda = +\pi/2$

$$\phi = (\Omega - 0.5)\,\pi \tag{51}$$

where Ω is in rev/sec. For $\lambda = -\pi/2$,

$$\phi = (\Omega - 1.5)\,\pi \tag{52}$$

Equations (51) and (52) show that the phase angles differ by 180° depending upon which thruster is fired. However, the phase angle of equation (51) can be used if the polarity of the accelerometer output is reversed for the alternate thruster. The nominal accelerometer location ϕ_A can be determined using equations (49) - (51). This angle is shown in line 16 of Table 1. Because of the value of k, $\phi_A \simeq \phi$.

Equation (42) gives the expression for the accelerometer gain. Since k (see line 7, Table 1) for the SAS-D spacecraft is close to one, equation (12) can be approximated by

$$a_0 \simeq (\omega_x^2 - \Omega)\,[y_0^2 + z_0^2]^{1/2}. \tag{53}$$

Letting $r = [y_0^2 + z_0^2]^{1/2}$, the output of the accelerometer is given by

$$a_x = (\omega_x^2 - \Omega^2)\, r\, \theta \sin(\Omega t + \phi), \tag{54}$$

where r is the radial placement of the accelerometer. This result is given in line 17, Table 1.

Rate Gyro. To detect nutation using a rate gyro consider a rate gyro mounted at an angle ϕ_{RG} from the principle y-axis. The measured angular rate is given by

$$\omega_M = \omega_y \cos\phi_{RG} + \omega_z \sin\phi_{RG}. \tag{55}$$

Using the results of equations (9) and (14), equation (55) becomes

$$\omega_M = A_y \sin \Omega t \cos \phi_{RG} + A_z \cos \Omega t \sin \phi_{RG} \tag{56}$$

Furthermore, using the results of equations (17) and (19) let

$$\omega_M = \omega_0 \theta \sin (\Omega t + \phi) \tag{57}$$

where

$$\omega_0 = [k^2 + 1] (\omega_x - \Omega) \tag{58}$$

and

$$\phi = \tan^{-1} \left[\frac{1}{k} \tan \phi_{RG} \right] \tag{59}$$

Now, by changing equation (57) to

$$\omega_M = \omega_0 \theta \sin (\Omega t + \mu) \tag{60}$$

the phase requirement analysis for the accelerometer is directly applicable to the rate gyro. Thus, equations (45) - (48) and (51) apply. Since $k \simeq 1$, $\phi_{RG} \simeq \phi$ from equation (59).

For the rate gyro, the gain from equation (58) is approximately $\sqrt{2}(\omega_x - \Omega)$. Thus, the output of the rate gyro is given by

$$\omega_M = \sqrt{2} (\omega_x - \Omega) \theta \sin (\Omega t + \phi). \tag{61}$$

The mounting angle and output are given in lines 18 and 19, Table 1.

Pre-Positioned Rate Gyro. Nutation can also be detected by a rate gyro positioned at any angle if the phase of the output is adjusted electronically. Considering that the y-axis rate gyro is used, equation (55) becomes

$$\omega_M = \omega_y \tag{62}$$

and equation (60) reduces to

$$\omega_M = -k\,(\omega_x - \Omega)\,\theta \sin(\Omega t - \pi/2 + \mu). \tag{63}$$

Since $\phi = 0°$ for the y-axis rate gyro, from equation (45)

$$-\pi/2 + \mu = 0 + \psi + \beta_T$$

or (64)

$$\mu = \pi/2 + \psi + \beta_T$$

Setting equation (46) and (60) equal

$$\lambda - \pi + \Omega\left(\frac{t_1 - t_0}{2}\right) = \pi/2 + \psi + \beta_T \tag{65}$$

$$\psi = \lambda - 3/2\,\pi + \Omega\left(\frac{t_1 - t_0}{2}\right) - \beta_T \tag{66}$$

Assuming $\beta_T = 0$ and $(t_1 - t_0) = 1$ second, for $\lambda = +\pi/2$,

$$\psi_{RG} = (\Omega - 1)\,\pi. \tag{67}$$

for $\lambda = -\pi/2$,

$$\psi_{RG} = \Omega\,\pi. \tag{68}$$

Equations (67) and (68) differ by 180°. The phase angle of equation (67) can be used for both thrusters if the polarity of the rate gyro is reversed. The phase angle in equation (67) is given in line 20, Table 1. The output of the rate gyro, from equation (63) is given in line 21, Table 1.

NUTATION CONTROL

In discussing a nutation control system it is worthwhile to consider the effects that nutations will have upon the SAS-D mission. Upon entering the transfer orbit the Delta vehicle spin stabilizes the SAS-D spacecraft so that

the apogee burn can be oriented properly for synchronous orbit insertion. Thrust misalignment and nutation tend to divert thrust so that the Δv imparted to the spacecraft for synchronous orbit insertion is not maximum. Considering the misalignment angle very small, the loss in Δv due to a nutation angle θ is given by

$$\delta \Delta v \simeq -\frac{\theta^2}{2} \Delta v. \tag{69}$$

Since synchronous orbit trim requires approximately one pound of hydrazine for each 3 m/sec correction in Δv, minimizing the nutation angle θ, in general, minimizes the hydrazine budget required for trim.

In some spacecraft the nutation angle must remain small so that ejection of the apogee kick motor will not strike the spacecraft structure. This is not a consideration for the SAS-D since the apogee kick motor will not be ejected.

The most significant reason for requiring a small nutation angle is apparent from equation (30). The smaller the initial nutation, the greater the time elapsed before the nutation builds up to a given level. Hence, nutation removal is required less frequently and hydrazine is conserved.

Grasshoff [1] describes a nutation control method in which the sinusoidal sensor output is compared against a threshold. The thruster is fired for the duration that the sensor output is greater than the threshold. Nutation is removed by a series of thrust pulses until the nutation is below the threshold. However, if a minimum thrust pulse length and/or secondary threshold are not employed, near the threshold the thrust pulse is so short that nutation removal and build up are equal and hydrazine is wasted. Furthermore, if the thrust pulse duration is not an integral multiple of the spin frequency period, the total momentum vector orientation is altered.

For the SAS-D spacecraft a more straightforward nutation control can be employed. In this case, each time the thruster is fired, it fires for the period of one spin cycle. Equations (29) and (30), repeated here for convenience, determine the nutation angle removed by one thrust pulse.

$$\Delta \omega_0 = \frac{2 N_0}{\Omega} \sin\left[\frac{\Omega (t_1 - t_0)}{2}\right]$$

$$\Delta \theta = \frac{-\Delta \omega_0}{\omega_x - \Omega}$$

Thus, for $(t_1 - t_0) = 1$ second, which is the nominal period for one spin cycle, $\Delta\theta_{\omega_x}$ can be calculated. See line 22, Table 1.

A $\Delta\theta_{\omega_x}$ of about 0.8° can be removed by a single thrust pulse of one spin cycle duration. Hence, the nutation control can be designed with a threshold $\theta_T = 0.8°$. Whenever the sensed nutation angle exceeds this threshold a thrust pulse of one spin cycle duration will be fired.

Once the type of nutation control described above is established two questions must be answered: What is the hydrazine budget required, and is it near optimal? To answer the first question equation (30) can be re-written as

$$T_N = \tau \ln\left(\frac{\theta_T}{\theta_0}\right) \tag{70}$$

Assume that the nutation threshold is set at $\theta_T = 0.8°$ and that the thrust pulse removes 90% of the nutation. Thus, $\theta_T = 0.8$, $\theta_0 = 0.08$ and their ratio is 10. Also consider that the transfer ellipse (segment A in Table 1) may last until 3rd apogee, which is approximately 28 hours. Furthermore, assume a conservative dissipation time constant $\tau = 1000$ seconds. From equation (70) the time between thrust pulses is $T_N = 2303$ seconds (see line 23, Table 1). Thus, 44 seconds of thrust are required for the 28 hour (maximum) transfer ellipse. Assumping the low duty cycle specific impulse of hydrazine to be 120 lbf-sec per lbm (see page 5-67, Phase A report [3]), the weight of fuel required for a 5-lb thruster is 1.833 pounds (see line 24, Table 1).

Lines 24 and 25 of Table 1 also show the time between thrust pulses and hydrazine required for segments B and C. Here it is assumed that $\tau = 500$, segment B lasts for one hour and segment C lasts for eight hours.

To answer the question about the optimality of the proposed nutation control system consider equation (28) which shows that maximum nutation angle is removed if the thrust pulse duration is one-half the period of the nutation frequency. A comparison of the nutation period (line 10, Table 1) with the one second period of the spin frequency indicates that the thrust pulse is applied for more than half the nutation period. Thus, the nutation control system is sub-optimal in terms of hydrazine fuel consumed.

The optimal nutation removal can be determined from equations (29) and (30) with $(t_1 - t_0) = 1/2\ T_\Omega$. These results are shown in line 25, Table 1. Comparing the proposed thrust duration with the optimum thrust duration $1/2\ T_\Omega$ (line 10, Table 1), it appears that about a 34% fuel waste occurs. However, since a thrust duration of one-spin cycle causes no change in the momentum

vector, and since the sub-optimal hydrazine budget is small, the proposed system is recommended.

Another advantage of the proposed nutation control system results from the behavior of the hydrazine thrusters. Considerable difference occurs between cold and hot hydrazine thrusters in terms of specific impulse and thrust pulse shape. With the proposed nutation control system, time between thrust pulses is at least 1152 seconds (see line 23, Table 1). Thus, the thrusters can be considered cold at each firing and the nutation control system does not need to be adaptive to hot thrusters.

Figure 2 shows a block diagram of the proposed nutation control system. The phase of the accelerometer or rate gyro output is set (by physical position or electronically) so that a thrust pulse of one spin cycle duration is activated if the nutation senses exceeds the threshold. The threshold is a critical parameter and depends upon the amount of nutation which can be removed during one spin cycle. Thus, the spacecraft spin must be sensed to determine the thrust pulse duration and threshold.

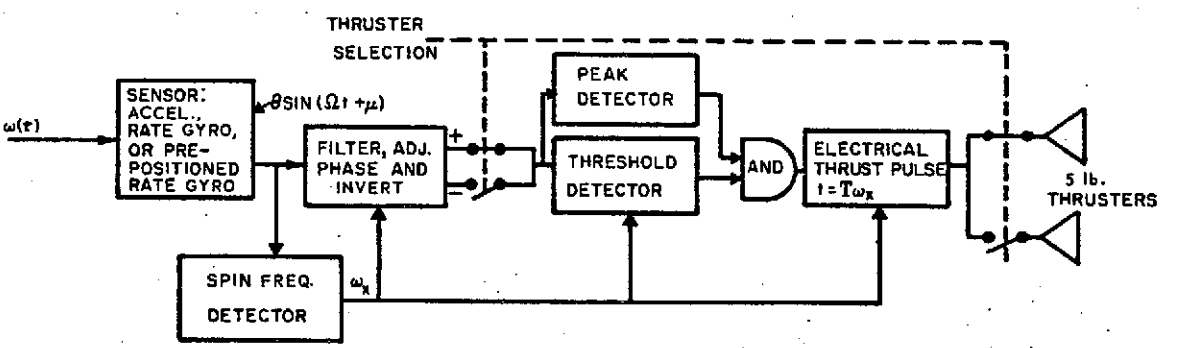

Figure 2. Nutation Control System.

Figure 3 shows the trajectory of the spin axis ω_x during nutation buildup and removal. The spin axis position spirals out until the threshold θ_T is reached. A properly phased thrust pulse is initiated which drives the spin axis to near zero.

A final question concerning the nutation control system needs to be answered. Considering the energy dissipation model of equation (30) and (31), how great can the nutation angle become before the nutation buildup exceeds the amount of nutation that can be removed? Equation (30) can be rewritten in the form

$$\theta_0 - \Delta\theta = \theta_0 \, e^{t/\tau}$$

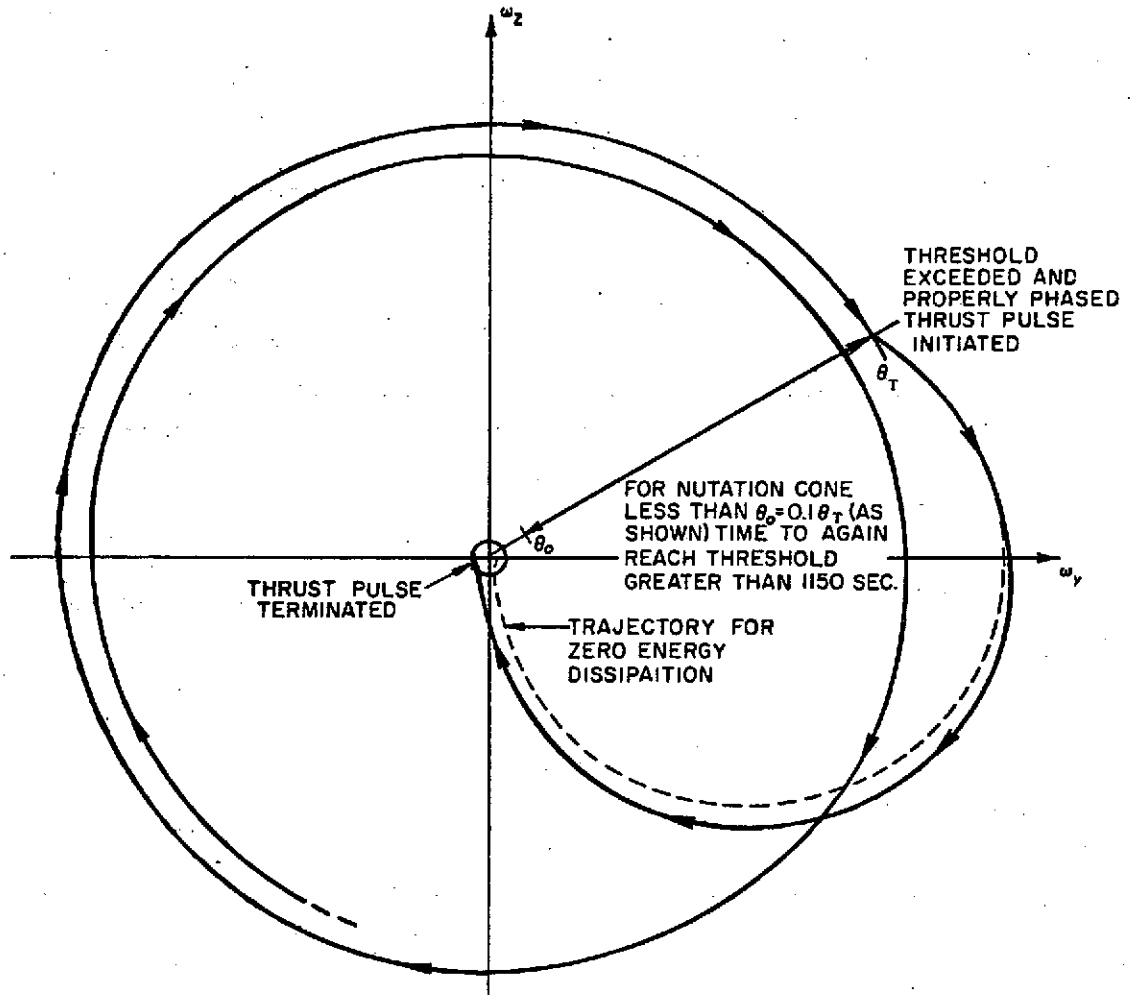

Figure 3. Trajectory of Spin Axis During Nutation Buildup and Removal.

where $\Delta\theta$ is the amount of nutation that can be removed by a thrust pulse and t is the nutation period. Then, the solution for $\theta_0 = \max \theta$ gives the nutation angle at which nutation due to dissipation equals nutation that can be removed. These results are given in lines 26 and 27, Table 1, for a thrust pulse of one spin cycle duration and for an optimum thrust pulse. Thus, for practical nutation angle limits of 15° - 30°, nutation removal is considerably greater than nutation due to energy dissipation.

ERROR ANALYSIS

In this section of the report it is worthwhile to look at an error analysis of the nutation control system. The two most important variables to investigate, in terms of error, are the nutation build-up due to energy dissipation and the amount of nutation removed per thrust pulse.

The nutation build-up due to energy dissipation will be analyzed first. The basic relationships are given in equations (30) and (70) and are repeated here for convenience.

$$\theta(t) = \theta_0 \, e^{t/\tau}$$

$$T_N = \tau \ln\left(\frac{\theta_T}{\theta_0}\right)$$

The time T_N between thrust pulses depends upon the energy dissipation time constant τ and the ratio of the threshold θ_T to the residual nutation θ_0 remaining after a thrust pulse. From equation (35), largest changes in τ result from errors in the inertia ratio. Changes in T_n due to changes in the amount of nutation removed per thrust pulse can be determined by a Taylor's series expansion and retention of the linear terms. The final result is

$$T_N = T_{N_0} \left[1 - 3\frac{\delta\sigma}{\sigma}\right]\left[1 - \left|\frac{1}{\ln\left(\frac{\theta_T}{\theta_0}\right)}\frac{\delta\theta}{\theta}\right|\right] \qquad (71)$$

For 90%, or better nutation removal per thrust pulse, $\ln(\theta_T/\theta_0)$ is greater than 2.3. Hence, a 10% error in the threshold setting results in about 5% decrease in the time between thrust pulses. Thus, 5% more hydrazine is required.

A larger effect occurs due to errors in the inertia ratio σ. As equation (71) shows, a 10% change in inertia ratio results in a 30% decrease in the time between thrust pulses.

Nutation removal will be discussed next. The basic relationships given in equations (29) and (30) are repeated here for convenience.

$$\Delta\omega_0 = \frac{2N_0}{\Omega} \sin\left[\frac{\Omega(t_1 - t_0)}{2}\right]$$

$$\Delta\theta = \frac{-\Delta\omega_0}{\omega_x - \Omega}$$

Changes in the amount of nutation removed can result from the thrust pulse duration ($t_1 - t_0$), the spin frequency ω_x, and the thrust magnitude N_0. Since thrust pulse duration is set as the period of one spin cycle, thrust pulse duration errors can be analyzed as spin frequency errors. Thus, the principal error sources are ω_x and N_0.

Combining equations (29) and (30) and expressing Ω as $\Omega(\omega_x)\,\omega_x$ (see line 6, Table 1); the expression for $\Delta\theta$ is given by

$$\Delta\theta = \frac{-2N_0 \sin\left[\frac{\Omega(\omega_x)\,\omega_x\,(t_1 - t_0)}{2}\right]}{(\Omega(\omega_x) - \Omega^2(\omega_x))\,\omega_x^2} \tag{72}$$

The change in $\Delta\theta$ due to changes in ω_x can now be determined from a Taylor's series expansion and retention of the linear terms. Thus,

$$\Delta\theta \simeq \Delta\theta_0 \left[1 - \left(1 - \Omega(\omega_x)\,\omega_x \left(\frac{t_1 - t_0}{2}\right) \cot\left[\Omega(\omega_x)\,\omega_x\left(\frac{t_1 - t_0}{2}\right)\right]\right)\frac{\delta\omega_x}{\omega_x}\right] \tag{73}$$

Letting $\omega_x\,(t_1 - t_0) = 2\pi$, the final result is

$$\Delta\theta \simeq \Delta\theta_0 \left[1 - 1.6\,\frac{\delta\omega_x}{\omega_x}\right] \tag{74}$$

Additional error analysis with respect to N_0 yields

$$\Delta\theta \simeq \Delta\theta_0 \left[1 + \frac{\delta N_0}{N_0}\right]\left[1 - 1.6\,\frac{\delta\omega_x}{\omega_x}\right] \tag{75}$$

From equations (71) and (75) it is evident that the time between thrust pulses T_n is sensitive to changes in the threshold and that the nutation removed per pulse $\Delta\theta$ is sensitive to changes in the spin frequency ω_x. Since the nutation control law is based on the fact that the threshold $\theta_T = \Delta\theta$, the nutation control must be adaptive to the spin frequency.

An error analysis must also be performed upon the output of the nutation sensor (accelerometer or rate gyro) since the output depends upon the spin frequency. From equations (54) and (58) it is evident that the amplitude of the sensor output varies with changes in the spin frequency. For the accelerometer the output change varies as twice the spin frequency change. For the rate gyro the variation is direct.

To summarize the results of the nutation control system error analysis, for the rate gyro sensor a 10% increase in spin frequency causes a 10% increase in the sensor output for a given nutation angle θ. In addition this change also causes a 16% decrease in the proper level of the threshold θ_T. The result is a threshold that is too low for the nutation removed by the thrust pulse and over correction occurs.

On the other hand, a 10% decrease in spin frequency causes a 10% decrease in the sensor output for a given nutation angle θ. In addition, this decrease also causes a 16% increase in the proper level of the threshold θ_T. The result is a threshold that is too high for the nutation removed by the thrust pulse and under correction occurs.

In either case, the ratio (θ_T / θ_0) in equation (70) is reduced and the time between thrust pulses T_n is diminished. The result is additional fuel consumption. Thus, the nutation control system, as shown in Figure 2, must be adaptive to the spin frequency.

Once system performance degradation due to spin frequency error has been eliminated the remaining error source is the thrust magnitude N_0. Considering the thrust magnitude to be known to within 10%, thrust errors will reduce the ratio (θ_T / θ_0) in equation (70) to 10 which is, in fact, the ratio that the nutation control system design is based upon. Thus, this error has been properly treated.

CONCLUSIONS

This report has described the analysis for the SAS-D nutation control system. The results are a control system design, predicated upon a conservative energy dissipation time constant, that provides properly phased thrust pulses of one spin cycle duration. Nutation is removed in a sub-optimal manner with respect to fuel consumed, but attitude errors are minimized. The analysis considers the possibility of sensing nutation via an accelerometer, a rate gyro, or a pre-positioned rate gyro.

The results of this study should be refined when a better knowledge of the spacecraft energy dissipation and hydrazine thrust pulse characteristics become available.

REFERENCES

1. Grasshoff, L. H., "An Onboard, Closed-Loop, Nutation Control System for a Spin-Stabilized Spacecraft," Journal Spacecraft And Rockets, pp. 530-535, May 1968.

2. Timoshenko, S. and Young, D., Advanced Dynamics, McGraw-Hill, 1948, pp. 335-341.

3. Phase A Report for Small UV Astronomy Satellite, Technical Plan, Goddard Space Flight Center, Greenbelt, Md., March 1971.

4. Fedor, J. V., Memo to Robert C. Baumann, "Recent Analytic Results from Fluid Slug Model for ATS-5 Heat Pipes," Goddard Space Flight Center, Greenbelt, Md., February 12, 1970.

5. Alfriend, K. T., "Analysis of a Partially Filled Viscous Ring Damper," NASA Technical Document X-732-71-456, Goddard Space Flight Center, Greenbelt, Maryland, October 1971.

6. Goldstein, H., Classical Mechanics, Addison-Wesley, 1959, pp. 161-175.